THESIS FOR THE DEGREE OF LICENTIATE OF ENGINEERING IN SOLID AND
STRUCTURAL MECHANICS

Crack growth paths in rolling contact fatigue – Numerical predictions

MOHAMMAD SALAHI NEZHAD

Department of Industrial and Materials Science
Division of Material and Computational Mechanics
CHALMERS UNIVERSITY OF TECHNOLOGY

Göteborg, Sweden 2022

Crack growth paths in rolling contact fatigue – Numerical predictions
MOHAMMAD SALAHI NEZHAD

Cover:
An illustration of a rail model subjected to thermal (T), contact (C) and bending (B) loads, and predicted crack paths for pure and combined loads [1].

Crack growth paths in rolling contact fatigue – Numerical predictions
MOHAMMAD SALAHI NEZHAD
Department of Industrial and Materials Science
Division of Material and Computational Mechanics
Chalmers University of Technology

ABSTRACT

Rolling contact fatigue (RCF) cracks in railway wheels and rails are costly and complex to deal with. Despite the extensive research efforts that have been put into understanding the mechanisms and developing appropriate predictive models for RCF crack growth, there are still a lot of open questions. This is the case regarding the direction and growth rate of RCF crack propagation under multiaxial wheel–rail contact loading, which also interplays with rail bending and thermal loads during the operational life of a rail.

In the first paper of this thesis (Paper A), a numerical procedure is developed to evaluate the effect of different operational loading scenarios on the predicted crack paths in rails. A 2D linear elastic finite element model of a rail part with an inclined surface-breaking crack has been implemented. The rail part is subjected to wheel–rail contact load, rail bending, and temperature drop as isolated scenarios and in combinations. The effective crack propagation direction is predicted based on an accumulative Vector Crack Tip Displacement (VCTD) criterion that accounts for crack face locking effects through a reversed shear threshold parameter. It has been shown that the crack path for combined thermal and contact loads varies gradually between the pure load cases while the combination of bending and contact loading has an abrupt change in predicted crack paths. Furthermore, the dependency of the results on the reversed shear threshold parameter is investigated.

The influence of crack face friction on the crack path is investigated in the second paper (Paper B). The numerical procedure developed in Paper A is utilised, and crack face friction is modelled by a Coulomb friction model. Qualitative predictions are obtained for varying magnitude of the coefficient of friction, as well as for varying parameters of the crack growth criterion. It is observed that the frictional crack tends to go deeper into the rail under a pure contact load and for a combination of bending and contact loads, while the friction has a moderate influence on the crack path for combined thermal and contact loads. Furthermore, assessment of the ranges of crack face deformation indicates that friction reduces the crack growth rate.

Keywords: Rolling contact fatigue, Crack propagation, Crack growth direction, Vector crack tip displacement, Crack face friction.

To my beloved wife, Maryam.

Preface

The following work was carried out between September 2019 and February 2022 at the Department of Industrial and Materials Science at Chalmers University of Technology within the research project MU38 "Growth of rolling contact fatigue cracks". The current study is part of the on-going activities within CHARMEC – Chalmers Railway Mechanics (`www.chalmers.se/charmec`). Parts of the study have been funded from the European Union's Horizon 2020 research and innovation programme in the project In2Track2 and In2Track3 under grant agreement Nos 826255 and 101012456.

Acknowledgements

First and foremost, I would like to thank my supervisors, Professor Fredrik Larsson, Professor Elena Kabo, and Professor Anders Ekberg for their endless support, great patience and encouragement, and excellent guidance. It was very pleasant and instructive for me to work with you and I am really looking forward to continuing the project with you all. Special thanks go to Dr. Dimosthenis Floros, who gave me a lot of help and support during the early stage of the project. I would also like to thank all my colleagues and friends at the divisions of Material and Computational Mechanics and Dynamics for making a joyful work environment.

Finally, I want to express my gratitude to my family for their love and support. Last but not least, my highest appreciation would go to my beloved wife Maryam, for her understanding, patience, and endless support.

Gothenburg, February 2022
Mohammad Salahi Nezhad

THESIS

This thesis consists of an extended summary and the following appended papers:

Paper A Mohammad Salahi Nezhad, Dimosthenis Floros, Fredrik Larsson, Elena Kabo, Anders Ekberg, Numerical predictions of crack growth direction in a railhead under contact, bending and thermal loads. *Engineering Fracture Mechanics* **261** (2022), p. 108218.

Paper B Mohammad Salahi Nezhad, Fredrik Larsson, Elena Kabo, Anders Ekberg, Influence of crack face friction on crack propagation in a railhead. *To be submitted for international publication.*

The appended papers were prepared in collaboration with the co-authors. The author of this thesis was responsible for the major progress of the work, i.e., took part in planning of the papers, developed the theoretical and computational framework, carried out numerical implementation and simulations and wrote major parts of the papers.

CONTENTS

Part I
Extended Summary

1 Introduction

1.1 Background and motivation

In recent decades, demands for rail transportation have been raised due to the high safety and very low environmental impact. Rail transports are about fifty to one hundred times safer than road transports [2] and have the lowest CO_2 emissions per passenger kilometer among the different means of transport (road, maritime, air and rail) [3]. Since the amount of available track increases at a slower rate than the transport volumes, availability for inspections and maintenance is decreasing while consequences of improper maintenance become larger and larger. Rolling Contact Fatigue (RCF) of rails, which is pervasive and very costly to mitigate, is a major issue influencing both the reliability and safety of the railways. For example, RCF defects in the European rail system were estimated to cost about 300 MEUR annually in 2000 [4]. The ability to understand and predict the behaviour of these defects, allowing for optimisation of rail maintenance, would be of outmost interest for rail managers.

Figure 1.1: *Gauge corner RCF cracks of a rail. Photo: Anders Ekberg.*

RCF cracks can grow either downwards into the railhead causing rail breaks, which are obvious safety risks, or towards the rail surface, which leads to spalling of the rail material. Modified contact conditions, which is a direct consequence of the spalling of the rail, can also change the dynamic response of the track. This may worsen the situation. The development of RCF cracks is a complex phenomenon to predict [5], and there are still many open questions especially regarding RCF crack propagation in the zone near the rail surface.

Three general questions are typically needed to be answered by a crack propagation prediction:

1. When is a crack (of a certain size and orientation) formed? (initiation)

2. In which direction does a crack tend to grow? (growth direction)

3. How fast does a crack propagate? (growth rate)

The focus of this research is on the crack growth direction (second question).

1.2   Aim of research

This research aims to improve the predictions of RCF crack growth in rails under operational loading scenarios. In particular, the goal is to predict growth paths for a propagating crack.

1.3   Scope and limitations

The focus of this work is on the prediction of crack growth paths using a 2D model of a rail with an isolated surface-breaking inclined RCF crack under a moving Hertzian contact load, a temperature drop and rail bending due to a passing wheelset, and combinations of these. The crack initiation stage is out of scope for this study, and the prediction of crack growth rate is mainly left for future investigations. In the model, the crack propagates in a linear elastic steel material. Thereby, the influence of the anisotropy existing at the rail surface is not considered in this research. It should be pointed out that the 2D model can only give qualititve predictions of crack growth. In future, a 3D modeling can help to investigate the problem in a more realistic manner, i.e. allowing for quantitative estimates of the contribution of the different loads. In a future 3D analysis, the model parameters can be calibrated towards data from field measurements.

1.4   Outline of the thesis

An overview of fatigue crack growth direction criteria under mixed-mode loading, with specifics of the employed criterion, is presented in Chapter 2. In Chapter 3, the numerical framework is introduced. Some of the main results are explained in Chapter 4. The summary of appended papers is given in Chapter 5. Finally, the main conclusions from the study, and some suggestions for future work are discussed in Chapter 6.

2 Prediction of fatigue crack growth direction under mixed-mode loading

2.1 Overview

Early crack growth investigations were done within the scope of Linear Elastic Fracture Mechanics (LEFM), see e.g. [6]. The most important assumption in LEFM is that the material response follows the linear elasticity theory. The loading of the crack can then be quantified by the Stress Intensity Factor (SIF), which was originally defined in [7]. Therefore, there are three independent modes of crack growth: opening mode (mode I, tensile-growth), sliding mode (mode II, shear-growth) and tearing mode (mode III, shear-growth). A crack can grow in one of these modes or their combinations. Abundant studies in the literature focus on the tensile-growth since the majority of the practical cases occurs in this mode. However, this is not the case for RCF cracks. The loading of such cracks are in general in mixed-mode. Conventionally, the criteria developed in the literature for fatigue crack growth direction under mixed-mode loading can be divided into three categories: stress-, energy- and displacement-based.

Stress-based criteria are typically developed based on the SIF concept. They generally presume small scale yielding at the tip of a relatively long crack (not interacting with the material microstructure) and proportional loading. Some of the most common of these criteria are Maximum Tangential Stress (MTS) [8], Maximum Shear Stress (MSS) [8] and Minimum Strain Energy Density (MSED)[1] [9] criterion. The range of SIFs are usually employed to adapt these originally developed criteria for static analysis to the fatigue crack growth, see e.g. MTSR (Maximum Tangential Stress Range) criterion as proposed in [10]. Different extensions of each of these criteria exist in the literature to account for different phenomena. For example, crack closure can be considered by applying effective SIFs, see e.g. [11]. Regarding the performance of these criteria, it has been shown that they typically give more reliable results when one mode dominates crack propagation. MTS- and MSED-based criteria have good accuracy for the predictions in mode I dominated crack growth [12] whereas their performance worsen as the crack shear loadings increase [13, 14]. On the other hand, MSS-based criteria can predict shear driven growth accurately [15] but are inaccurate for tensile growth [16].

Energy-based criteria set out from the energy release rate, which was defined in [17] as the rate of change in potential energy with respect to an increase of the crack area. Also, the term crack driving force is commonly used in the literature as the sensitivity of the energy with respect to a crack extension. These criteria usually employ a measure called the J-integral [18, 19]. Although this has originally been proposed for the non-linear elastic case in [19], it can to some extent be applicable also to the elastic-plastic conditions. A cyclic J-integral (ΔJ) that considers elastic-plastic responses can be employed for fatigue crack growth, see e.g. [20, 21]. This criterion can (to some extent) deal with multiaxial loading but it does not in itself provide any information on growth directions. During the recent decades, the concept of the Configurational Forces (CF) (or material forces) [22] was adapted to evaluate crack driving forces [23]. In this approach, the crack driving force can give information about both rate and direction of crack growth. Thus, it

---

[1]Note that, the MSED criterion was originally defined as an energy-based criterion but since its strain energy was defined as a function of SIFs, it is mentioned here.

attracted great attention from the researchers in the field of the crack propagation. A framework for RCF crack propagation using a CF criterion developed in [24] has shown that the perpendicular component of the employed CF criterion is heavily path-dependent. A CF criterion considered in [16] to simulate four mixed-mode fatigue crack growth experiments. It has illustrated that the performance of the criterion decreases as shear loading increases. It is also sensitive to the material model used in the simulations, and the approach for the evaluation of crack driving force (i.e. viscous or rate-independent).

Displacement-based criteria are developed based on the crack face displacements near the crack tip, i.e. crack tip opening displacement (δ_I) and crack tip sliding displacement (δ_II). Due to difficulties in measuring δ_I and δ_II and other complicating factors, there are very few displacement-based criteria in the literature for mixed-mode loading [25]. For LEFM, the δ_I and δ_II are related to SIFs. In a general case, the procedure is also applicable to, e.g., elastic-plastic response since the criterion is only dependent on the δ_I and δ_II. However, the criterion is sensitive as to how δ_I and δ_II are evaluated. The analytical predictions of the Vector Crack Tip Displacement (VCTD) criterion show good agreement with experimental results under proportional mixed-mode loading [26]. In simulating four fatigue tests in [16], a modification of the VCTD criterion yielded promising results for a linear elastic material model and it was also shown that modelling the cyclic elastic–plastic material response does not improve the predictions' accuracy by the criterion. However, the criterion has not been investigated for operational wheel–rail loading conditions.

Based on the above discussion and the challenges mentioned in [27, 28], there are still some issues regarding the fatigue crack growth under mixed-mode loading which are not fully addressed in the literature. The situation is complex for RCF cracks [5] since the (frictional) rolling contact conditions impose a non-proportional multiaxial stress/strain state, which exerts compression and mixed-mode deformations on these cracks. In addition, the formation of large plastic deformation is present near the contact surfaces. Since displacement-based criteria do not have any limiting theoretical assumption in order to be applicable for RCF cracks and they have shown promising results [16, 29], the VCTD criterion has been chosen for the investigations in this research.

2.2 The VCTD criterion

The VCTD criterion [26] was originally proposed based on the assumption that the microscopic mechanism for fatigue crack growth is cyclic deformations. Hence, it was concluded that the crack tip displacements represent the condition at the crack tip and can be used to define the propagation.

As elaborated in **Paper A**, the fatigue crack growth direction in the VCTD criterion [26] is determined in the crack local coordinate system originated in the crack tip and shown in Fig. 2.1a, as $\vartheta = \arcsin(\Delta\delta_\mathrm{II}/\Delta\delta)$, where $\Delta\delta = \sqrt{\Delta\delta_\mathrm{I}^2 + 2\Delta\delta_\mathrm{I}\Delta\delta_\mathrm{II} + 2\Delta\delta_\mathrm{II}^2}$.

In this study, the VCTD criterion is modified (see [16]) to account for non-proportional loading, and implemented as follows:

1. $\delta_\mathrm{I}(t)$ and $\delta_\mathrm{II}(t)$ are computed at each time instance t of the load cycle at a constant (small) distance d_h, see Fig. 2.1.

2. Using $\overline{\delta}_\mathrm{I/II} = \frac{1}{2}\left[\max_t\left(\delta_\mathrm{I/II}(t)\right) + \min_t\left(\delta_\mathrm{I/II}(t)\right)\right]$, the "amplitudes" of $\delta_\mathrm{I}(t)$ and $\delta_\mathrm{II}(t)$ are
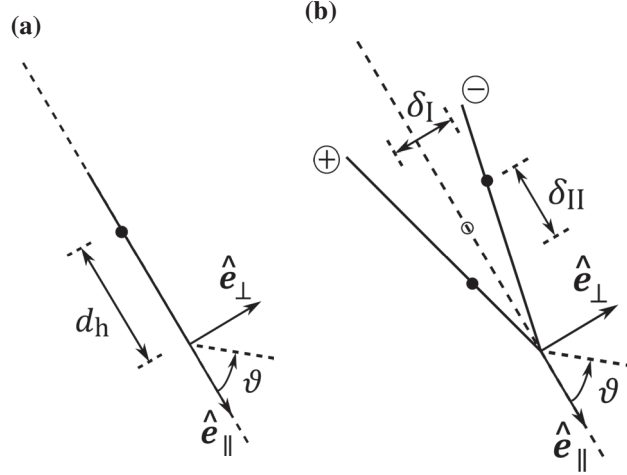
Figure 2.1: *(a) Undeformed closed crack. (b) Crack tip displacements illustration. The dashed line indicates the orientation of the undeformed crack [1].*

defined as

$$\tilde{\delta}_{\mathrm{I/II}}(t) = \delta_{\mathrm{I/II}}(t) - \overline{\delta}_{\mathrm{I/II}} \tag{2.1}$$

"Amplitudes" are here employed to account for kinematic hardening effects due to local plasticity at the crack tip.

3. Similar to [26], the instantaneous crack driving displacement, $\tilde{\delta}(t)$, and the instantaneous crack growth direction in the local coordinate system as in Fig. 2.1a, $\vartheta(t)$, are defined as[2]

$$\tilde{\delta}(t) = \sqrt{\langle \tilde{\delta}_{\mathrm{I}}(t)\rangle^2 + 2\langle \tilde{\delta}_{\mathrm{I}}(t)\rangle|\tilde{\delta}_{\mathrm{II}}(t)| + 2\tilde{\delta}_{\mathrm{II}}(t)^2}, \tag{2.2}$$

and

$$\vartheta(t) = \arcsin \frac{\tilde{\delta}_{\mathrm{II}}(t)}{\tilde{\delta}(t)}. \tag{2.3}$$

4. The crack driving displacement for the entire load cycle is determined by

$$\Delta \mathbf{a} = \underset{\Delta \tilde{\mathbf{a}} \in \{\Delta \mathbf{a}^+, \Delta \mathbf{a}^-\}}{\mathrm{argmax}} \|\Delta \tilde{\mathbf{a}}\|, \tag{2.4}$$

where $\Delta \mathbf{a}^+$ and $\Delta \mathbf{a}^-$ are the trial crack driving displacements for presumed positive and negative growth directions, respectively, defined as

$$\Delta \mathbf{a}^{+/-} = \int_0^{T_c} \delta \mathbf{a}^{+/-}(t)\,\mathrm{d}t, \quad \delta \mathbf{a}^{+/-}(t) = \langle \mathrm{d}_t \tilde{\delta}(t)\rangle \hat{\mathbf{e}}_\vartheta(t) f^{+/-}(t), \tag{2.5}$$

where $\delta \mathbf{a}^+(t)$ and $\delta \mathbf{a}^-(t)$ are the instantaneous trial crack driving displacements for presumed positive and negative growth directions, respectively. They are here defined based on the 'rate-independent' response and with

$$f^+(t) = \begin{cases} 0 & \tilde{\delta}_{\mathrm{II}} < 0 \text{ and } \frac{\delta_{\mathrm{I}}}{|\delta_{\mathrm{II}}|} \leq \psi \\ 1 & \tilde{\delta}_{\mathrm{II}} \geq 0 \text{ or } \frac{\delta_{\mathrm{I}}}{|\delta_{\mathrm{II}}|} > \psi \end{cases}, \quad f^-(t) = \begin{cases} 0 & \tilde{\delta}_{\mathrm{II}} > 0 \text{ and } \frac{\delta_{\mathrm{I}}}{|\delta_{\mathrm{II}}|} \leq \psi \\ 1 & \tilde{\delta}_{\mathrm{II}} \leq 0 \text{ or } \frac{\delta_{\mathrm{I}}}{|\delta_{\mathrm{II}}|} > \psi \end{cases}, \tag{2.6}$$

---

[2]Here, the Macaulay brackets are introduced as $\langle \bullet \rangle = \frac{1}{2}[\bullet + |\bullet|]$

where ψ is a reversed shear threshold parameter, which is used to account for crack face locking by restricting the contribution of reversed shear instances. Here, crack face locking is defined as in [30], meaning that a part of the crack is active (has slip between crack faces) at each time instant and there are no relative displacements between the closed crack faces for inactive part(s) of the crack. Also, 'reversed shear' refers to a shear deformation with the opposite sign to the presumed growth direction.

5. The growth direction ϕ predicted for the entire load cycle in the local coordinate system of Fig. 2.1a is defined by the following unit vector,

$$\hat{\mathbf{e}}_\phi = \frac{\Delta \mathbf{a}}{\|\Delta \mathbf{a}\|}. \tag{2.7}$$

Remark: The formulation in Eq. (2.5) results in a rate-independent formulation related to the range of $\tilde{\delta}$. As an illustration, in the scalar case (considering constant direction),

$$\int_0^{T_c} \langle \mathrm{d}_t \tilde{\delta}(t) \rangle \, \mathrm{d}t = \max_{0 < t < T_c} \left(\tilde{\delta}(t) \right) - \min_{0 < t < T_c} \left(\tilde{\delta}(t) \right) = \Delta \tilde{\delta}. \tag{2.8}$$

Hence, the loading is proportional to the range $\Delta \tilde{\delta}$ and independent of the duration of the load cycle , T_c.

3 Numerical framework

3.1 Finite element model

In the finite element model, a rectangular (rail) part with the width of $w = 300\,\text{mm}$ and the height of $h = 100\,\text{mm}$ having an isolated surface-breaking inclined crack is used as a 2D representation of a rail, see Fig. 3.1. An initial crack with an inclination of $\varphi_0 = -25°$ and an initial crack length of $a_0 = 4.3\,\text{mm}$ with the tip initially at a depth of $d = 2\,\text{mm}$ is introduced. The crack is modelled as a discrete crack. To apply the contact constraints at the crack faces in the normal and tangential directions, a penalty formulation is employed. A Coulomb friction model is used to model the tangential behaviour. In this model, the tangential traction between two contacting surfaces is evaluated as

$$\begin{cases} |p_t| \leq \mu_{CF} p_n & v_t = 0 \ \ (\text{stick condition}) \\ p_t = -\mu_{CF} p_n \frac{v_t}{|v_t|} & v_t \neq 0 \ \ (\text{slip condition}) \end{cases}. \tag{3.1}$$

Here, μ_{CF} and p_n are the friction coefficient and normal contact pressure between the surfaces, respectively, and v_t shows relative sliding velocity.

Three-noded (linear) triangular elements featuring mesh refinement close to the crack tip are employed. No special or singular elements around the crack tip are incorparated in the model. Plane strain conditions are presumed and a linearly elastic material model is used.
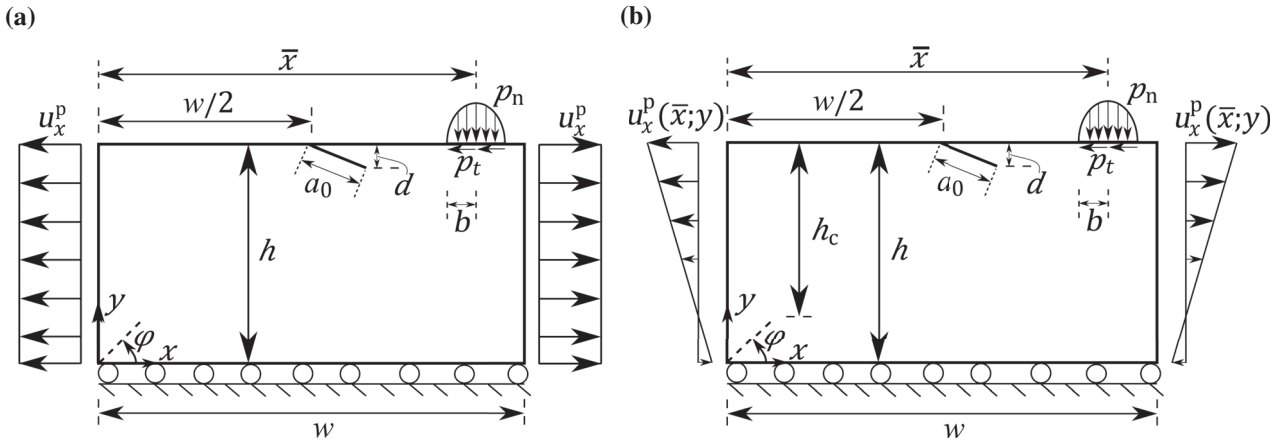

Figure 3.1: *A sketch of a 2D rail part with an isolated surface-breaking inclined crack subjected to a Hertzian contact load (p_n, p_t) and, (a) constant longitudinal prescribed displacements u_x^p, or, (b) boundary displacements $u_x^p(\bar{x}; y)$ corresponding to bending [1].*

3.2 Load scenarios

The influence of three load scenarios are considered: contact loading due to the passage of a wheel along the rail surface, and longitudinal thermal and bending loading employed as prescribed displacements acting on the side edges of the rail part. The employed boundary conditions corresponding to each of these loads are shown in Fig. 3.1. These load cases are briefly explained

7

below. The influence of each loading scenario on predicted crack path is evaluated independently and in combinations.

- **Contact load**

A traction, consisting of a frictional load associated with a pressure load, acts at the rail surface as a wheel passes along the rail. Using Hertzian contact theory, the contact pressure distribution along the top surface of the rail corresponding to the 2D contact load per thickness, P, is expressed for a given wheel load position, $\bar{x}$, [31] as

$$p_{\mathrm{n}}(\bar{x};x) = \frac{2P}{\pi b^2} \sqrt{b^2 - [x - \bar{x}]^2} \quad \text{for } |x - \bar{x}| < b. \tag{3.2}$$

The semi-axis of the contact patch, b, corresponding to the contact load P is evaluated using

$$b = \sqrt{\frac{4PR}{\pi E^*}}, \tag{3.3}$$

where R is the radius of the wheel and E^* is the effective elastic modulus of the wheel and the rail determined as

$$\frac{1}{E^*} = \frac{1 - v_{\mathrm{r}}^2}{E_{\mathrm{r}}} + \frac{1 - v_{\mathrm{w}}^2}{E_{\mathrm{w}}}. \tag{3.4}$$

Here, E denotes the elastic modulus and v is the Poison's ratio. Subscripts r and w indicate the rail and wheel materials, respectively.

Wheel–rail frictional stress distribution presuming full slip conditions are applied as $p_{\mathrm{t}}(\bar{x};x) = f_{\mathrm{wr}}\, p_{\mathrm{n}}(\bar{x};x)$, where f_{wr} is the traction coefficient.

- **Rail bending load**

A passing wheelset induces bending in the rails. By using the results of the in-house vertical dynamic vehicle–track interaction analysis code, DIFF [32], the evolution of bending moment over time at the crack mouth due a moving wheel load for a 6 m track section is presented in Fig. 3.2. The corresponding boundary displacements for a rail section of length w are obtained using the bending moment in rail, $M(\bar{x})$, see e.g. Fig. 3.2, and the moment–curvature relation for an Euler-Bernoulli beam [33] as

$$u_x^{\mathrm{p}}(\bar{x};y) = \frac{M(\bar{x})\,[y - [h - h_{\mathrm{c}}]]\,w}{2E_{\mathrm{r}}\,I_z}, \tag{3.5}$$

where h and h_c are geometrical parameters shown on Fig. 3.1b and I_z is the area moment of inertia of the rail profile.

- **Thermal load**

A continuously welded rail will experience thermal loads due to the variation, ΔT, of the ambient temperature from the stress free temperature. The equivalent thermal displacement at the edges of a rail section of length w using linear thermoelasticity assumption is evaluated [33] as

$$u_x^{\mathrm{p}} = -\alpha \Delta T \frac{w}{2}, \tag{3.6}$$

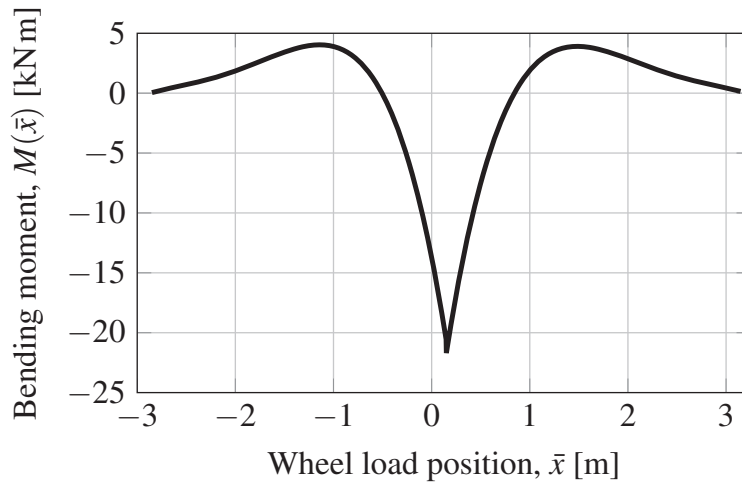where α is the thermal expansion coefficient.

Figure 3.2: *Illustration of the evolution of bending moment at the position of the crack as a function of the relative position of the wheel [1]. Simulation results from [32].*

3.3 Simulation of crack growth

Each load cycle is simulated using the finite element method, and the crack growth direction is predicted using the accumulative VCTD criterion described in Section 2.2. The accumulated growth for multiple cycles is simulated by propagating the discrete crack in the predicted direction and repeat the process.

In this study, the rate of propagation is not predicted. Therefore, the length of the incremental propagation of the crack is a pure discretisation parameter (rather than representing a certain number of load cycles).

4 Analyses and results

4.1 Preliminaries

The numerical model of the rail part described in Chapter 3 was implemented in the commercial Finite Element (FE) software ABAQUS/CAE [34]. A MATLAB [35] code was developed to predict the crack growth direction using the modified VCTD criterion detailed in Section 2.2. The analyses featured unbiased crack propagation based on the predicted growth direction at the end of each load cycle with the growth increment of 0.2 mm, as discussed in Section 3.3. The crack paths presented in the following sections were evaluated after three growth increments. Different FE meshes with the element size from 24 μm to 8 μm near the crack tip considered in the mesh sensitivity analyses, see the discussion in **Paper A**. Therefore, a mesh with the element size of 17 μm near the crack tip was chosen as the mesh size for the following results.

4.2 Highlighted results for frictionless cracks

4.2.1 Combined thermal and contact load

To model the crack growth under winter conditions in rails, boundary displacements corresponding to a temperature of $\Delta T = -20\,°\mathrm{C}$ was applied to the model in Fig. 3.1a in combination with a moving Hertzian contact load of different magnitudes and a traction coefficient of $f_{\mathrm{wr}} = 0.3$. The predicted crack paths for the studied load combinations are shown in Fig. 4.1 for $\psi = 0.001$ and $\psi = 0.01$. It is seen that the crack tends to grow towards a shallower path as the contact load magnitude increases. This takes place gradually and is motivated by the fact that the contribution of the contact load to the total load increases. Results have the same trend for both ψ values, it is thus concluded that the employed ψ value does not have a strong influence on the characteristics of the predicted crack path for these load combinations.
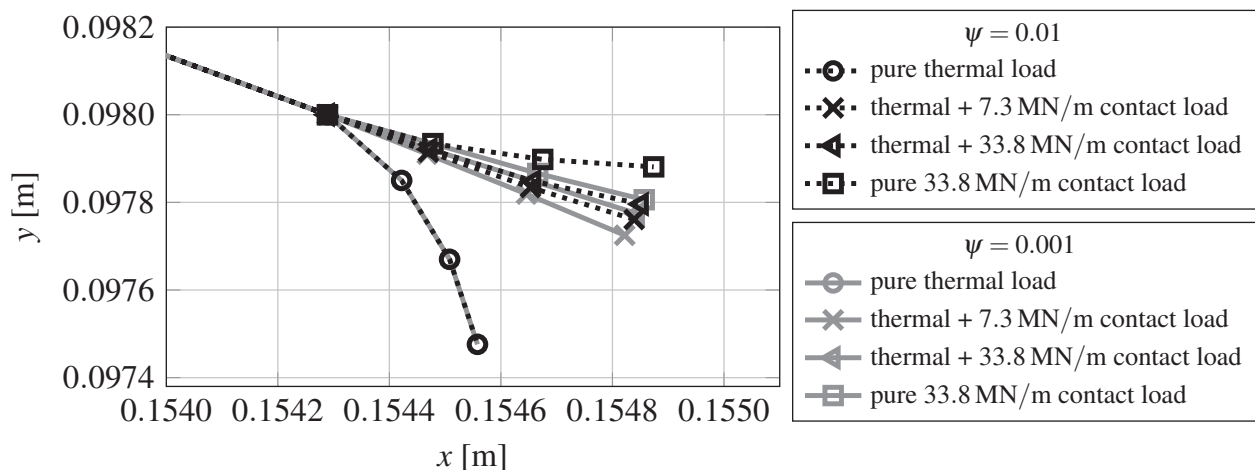

Figure 4.1: *Predicted crack paths under combined thermal and contact loads for a frictionless crack [1].*

4.2.2 Combinations of bending and contact load

To mimic the bending of rail by the passing wheels, the model in Fig. 3.1b was loaded with boundary displacements corresponding to a bending moment (see Fig. 3.2), and a moving contact load of varying magnitude with a traction coefficient of $f_{wr} = 0.3$. The predicted crack paths for the investigated load combinations are illustrated in Fig. 4.2 for $\psi = 0.001$ and $\psi = 0.01$. It is observed that the combinations of bending and low contact loads result in crack path predictions similar to those of pure bending, while the predicted crack paths for higher contact loads in combination with bending are closer to the crack path for a pure contact load. The trends are similar between $\psi = 0.001$ and $\psi = 0.01$, however, the jump between the paths occurs at a lower contact load for $\psi = 0.001$. This shows that the predicted crack path for combined bending and contact loads are somewhat sensitive to the employed ψ value.
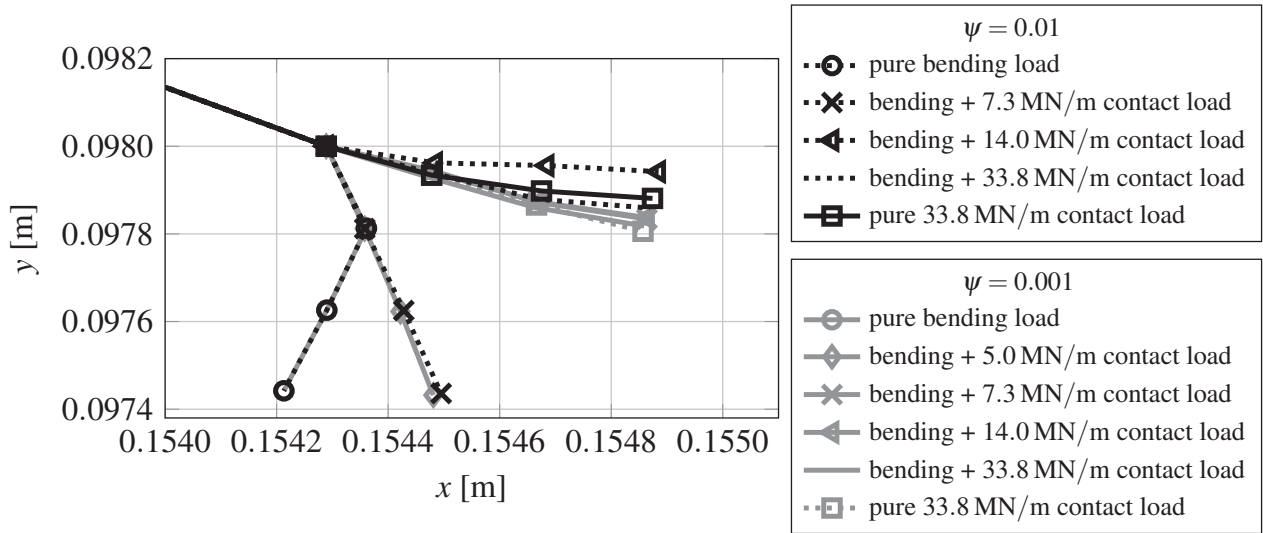

Figure 4.2: *Predicted crack paths under combinations of bending and contact load for a frictionless crack.*

4.3 Highlighted results for frictional cracks

4.3.1 Combined thermal and contact load

Load combinations as described in Section 4.2.1 were employed to investigate the influence of the crack face friction on the crack growth. The predicted crack paths for frictional and frictionless cracks are shown in Fig. 4.3. Here, the reverse shear condition in the criterion was removed and $\bar{\delta}$ was evaluated solely from the pure contact load part of each load combination, see discussion in **Paper B**. The trend of the results is the same for both cases with a little more deviation towards transverse growth for the thermal and $7.3\,\text{MN/m}$ contact load in the frictionless crack. It is thus concluded that the crack face friction has a moderate influence on the predicted crack path. Initial investigations of the crack face displacements near the crack tip (not shown here, see **Paper B**) showed that the friction is expected to reduce the crack growth rate.
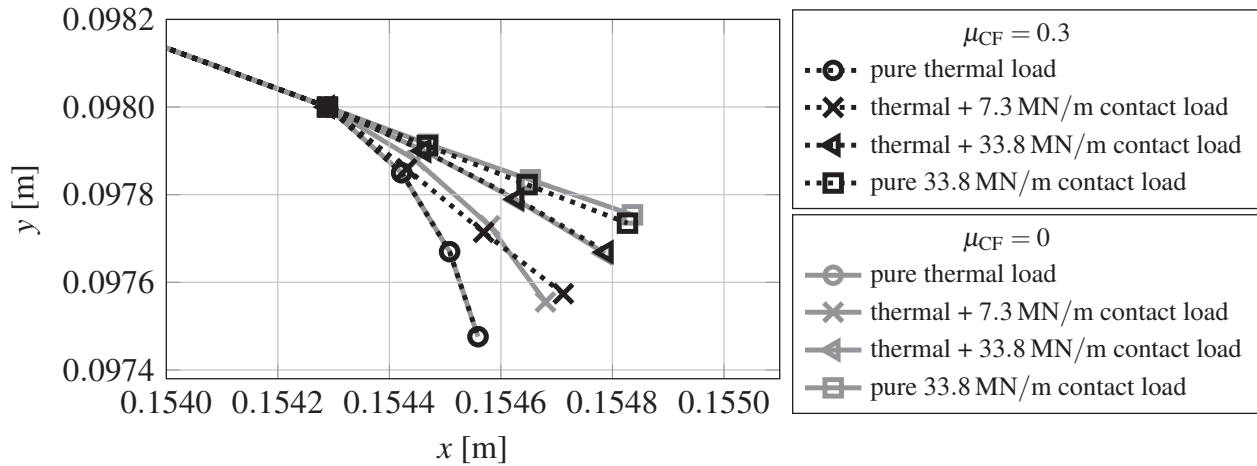
Figure 4.3: *Predicted crack paths under combined thermal and contact loads with neglecting the reversed shear condition and evaluating δ̄ solely from the pure contact load part of each of the considered combined load in the criterion.*

4.3.2 Combinations of bending and contact load

In order to study the influence of the crack face friction on the crack growth under these load combinations, the similar load cases as described in Section 4.2.2 were employed to the model in Fig. 3.1b for frictional and frictionless cracks. The predicted crack paths for neglecting the reverse shear condition in the criterion are presented in Fig. 4.4. The crack grows deeper into the rail in the presence of crack face friction for this load combination, and the friction has more pronounced influence on the predicted crack path when the bending load is combined with the lower contact load. Similar to the combined thermal and contact load in Section 4.3.1, initial investigations on the crack face deformation near the crack tip indicated that the frictional crack seems to propagate slower into the rail.
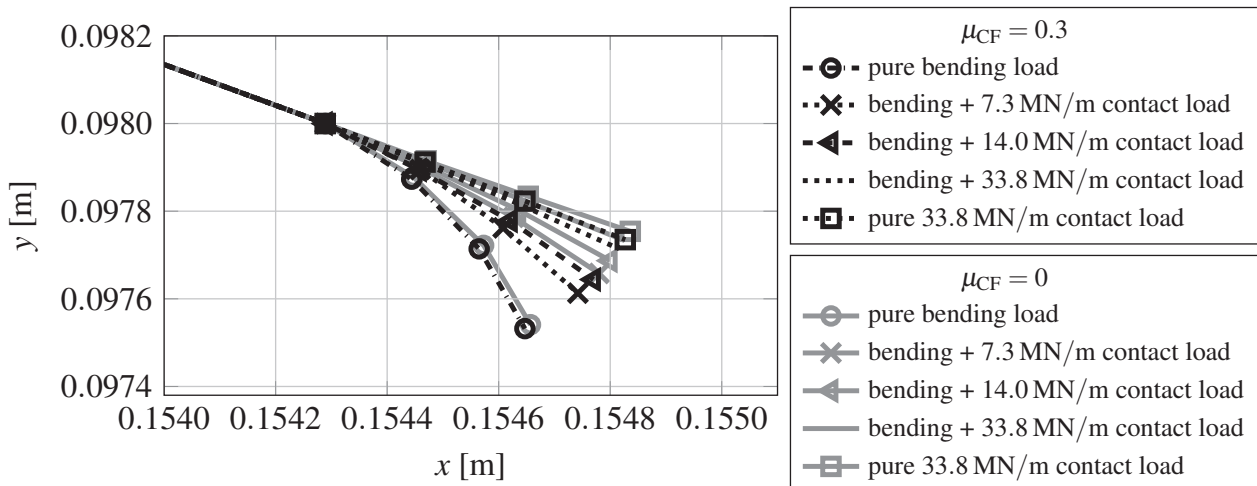

Figure 4.4: *Predicted crack paths under combinations of bending and contact load with neglecting the reversed shear condition in the criterion.*

5 Summary of appended papers

5.1 Paper A: Numerical predictions of crack growth direction in a railhead under contact, bending and thermal loads

A numerical framework for predicting RCF crack growth directions under different operational load conditions has been developed and implemented for a 2D linear elastic model of a rail with an isolated surface-breaking frictionless crack. The inclined crack is propagated into the rail in an unbiased manner (i.e. not following a prescribed path). The crack growth direction is predicted using an accumulative VCTD criterion. The influence of crack face locking is considered by introducing a reversed shear threshold parameter, ψ. It has been shown that when thermal load combines with the contact load, the crack path is changed gradually between the pure load cases, while there is an abrupt variation in the crack path for combinations of bending and contact load. The effect of the employed ψ value on the predicted crack path is investigated.

5.2 Paper B: Influence of crack face friction on crack propagation in a railhead

A numerical procedure to simulate frictional RCF crack growth under different operational scenarios in a 2D model of a rail has been developed. An isolated surface-breaking inclined crack has been embedded into the rail, which was assumed to have a linear elastic material under plane strain conditions. The crack face friction has been modelled using a Coulomb friction model. Qualitative predictions are obtained for varying magnitude of the coefficient of friction, as well as for varying parameters of the crack growth direction criterion, which is an accumulated VCTD. It is found that the frictional crack tends to go deeper into the rail under pure contact load and combinations of the bending and contact load while the friction has a moderate influence on the crack path for combined thermal and contact loads. Also, assessment of the ranges of the VCTD components indicates that a frictional crack is expected to have a lower growth rate.

6 Conclusions and future work

This research deals with predicting unbiased RCF crack propagation under operational loads pertaining to rail applications through numerical simulations. To this aim, the numerical framework briefly discussed in Chapter 3 in combination with an accumulative VCTD criterion, that can account for crack face locking through the introduction of a reversed shear threshold parameter, has been employed. The conclusions regarding the predicted growth of a frictionless RCF crack under combined loads (**Paper A**) are as follows:

- At the presence of contact and thermal loads, the predicted crack path is found to change gradually from transverse growth, corresponding to pure thermal loading, to shallow growth, corresponding to a pure contact load.

- For the combined bending and contact loads, there is an abrupt variation in the predicted crack growth direction as the contact load is increased.

- The predicted final growth direction is almost insensitive to the size of the growth increment in the numerical procedure. The growth direction converges towards the final direction after a few load cycles.

- Predicted crack paths for pure contact load, and for combined bending and contact loads, are found to be moderately sensitive to the employed value of the ψ parameter.

Crack face friction is modelled using Coulomb friction and investigated in **Paper B** for the same combined load scenarios as investigated in **Paper A**. A few modifications are also investigated for the crack growth direction criterion. The following conclusions are obtained regarding the influence of friction:

- Crack face friction has a moderate influence on the predicted crack paths under combined thermal and contact load by neglecting the reverse shear condition and evaluating $\bar{\delta}$ solely based on the pure contact part of each of these combined loads in the criterion.

- The frictional crack tends to grow deeper into the rail under pure contact load and combinations of bending and contact load when neglecting the reverse shear condition in the criterion.

- Assessment of the ranges of the VCTD components indicates that crack face friction is expected to reduce the rate of crack propagation.

Several open questions regarding RCF crack propagation remain. Some of these are:

- Performing a parametric study on the influence of different modelling and loading parameters would be essential to understand the limitations and sensitivities of the developed numerical procedure, as well as to give a more thorough perspective on the influence of different loads on predicted RCF crack paths. Aforementioned conclusions were drawn based on the results pertinent to the limited number of studied load conditions. However, it is clear that the "best" formulation of the reversed shear condition in the criterion is still an open question that deserves further studies.

- Predicting crack growth rates cannot be addressed before having a robust predictive tool for simulating growth direction. The reason is that the growth direction governs the contribution of each mode to the loading of propagating cracks.

- Modelling a crack in a 3D rail should be investigated in order to study the problem in a more realistic manner. A 2D model of the rail cannot be a fully representative of a 3D rail in reality especially regarding the load conditions and crack geometry. For example, it is not possible in the 2D approximation to quantify the actual (3D) wheel–rail contact load that corresponds to the jump in the predicted crack path for combinations of bending and contact load. A 3D model also gives an opportunity to calibrate the model parameters towards experiments or data from field measurements.

- Investigating the influence of the material anisotropy and inelasticity that exists in a layer close to the rail surface on the growth of surface-breaking cracks will increase the understanding of the crack loading. This can be done via considering a proper plastic material model and developing a more generally applicable crack growth criterion.

References

[1] M. Salahi Nezhad, D. Floros, F. Larsson, E. Kabo, and A. Ekberg. Numerical predictions of crack growth direction in a railhead under contact, bending and thermal loads. *Engineering Fracture Mechanics* **261** (2022), p. 108218.

[2] *SIKA Basfakta 2008 – Övergripande statistik om transportsektorn, 2009:28 (in Swedish)*. Statens institut för kommunikationsanalys (SIKA), 2009, 125 p.

[3] C. Doll, C. Brauer, J. Köhler, and P. Scholten. *Methodology for GHG Efficiency of Transport Modes*. Fraunhofer-Institute for Systems and Innovation Research ISI, 2020, 88 p.

[4] E. E. Magel. *Rolling contact fatigue: A comprehensive review*. US Department of Transportation, Federal Railroad Administration, 2011, 132 p.

[5] A. Ekberg and E. Kabo. Fatigue of railway wheels and rails under rolling contact and thermal loading – an overview. *Wear* **258**.7–8 (2005), pp. 1288–1300.

[6] P. Paris and F. Erdogan. A critical analysis of crack propagation laws. *Journal of Basic Engineering* **85**.4 (1963), pp. 528–533.

[7] G. R. Irwin. Analysis of stresses and strains near the end of a crack traversing a plate. *Journal of Applied Mechanics* **24**.3 (1957), pp. 361–364.

[8] F. Erdogan and G. C. Sih. On the crack extension in plates under plane loading and transverse shear. *Journal of Basic Engineering* **85**.4 (1963), pp. 519–525.

[9] G. C. Sih. Strain-energy-density factor applied to mixed mode crack problems. *International Journal of Fracture* **10**.3 (1974), pp. 305–321.

[10] P. Dahlin and M. Olsson. The effect of plasticity on incipient mixed-mode fatigue crack growth. *Fatigue & Fracture of Engineering Materials & Structures* **26**.7 (2003), pp. 577–588.

[11] A. Abdel Mageed and R. Pandey. Fatigue crack closure in kinked cracks and path of crack propagation. *International Journal of Fracture* **44**.1 (1990), pp. 39–42.

[12] S. Biner. Fatigue crack growth studies under mixed-mode loading. *International Journal of Fatigue* **23**.Supplement 1 (2001), pp. 259–263.

[13] A. Abdel Mageed and R. Pandey. Mixed mode crack growth under static and cyclic loading in Al-alloy sheets. *Engineering Fracture Mechanics* **40**.2 (1991), pp. 371–385.

[14] A. Abdel Mageed and R. Pandey. Studies on cyclic crack path and the mixed-mode crack closure behaviour in Al alloy. *International Journal of Fatigue* **14**.1 (1992), pp. 21–29.

[15] P. E. Bold, M. W. Brown, and R. J. Allen. Shear mode crack growth and rolling contact fatigue. *Wear* **144**.1 (1991), pp. 307–317.

[16] D. Floros, A. Ekberg, and F. Larsson. Evaluation of crack growth direction criteria on mixed-mode fatigue crack growth experiments. *International Journal of Fatigue* **129** (2019), p. 105075.

[17] G. R. Irwin. Fracture strength relative to onset and arrest of crack propagation. *Proceedings oF ASTM* **58** (1958), pp. 640–657.

[18] G. Cherepanov. Crack propagation in continuous media. *Journal of Applied Mathematics and Mechanics* **31**.3 (1967), pp. 503–512.

[19] J. R. Rice. A path independent integral and the approximate analysis of strain concentration by notches and cracks. *Journal of Applied Mechanics* **35**.2 (1968), pp. 379–386.

[20] N. E. Dowling and J. A. Begley. Fatigue crack growth during gross plasticity and the J-Integral. *ASTM special technical publications* (1976), pp. 82–103.

[21] T. Hoshide and D. Socie. Mechanics of mixed mode small fatigue crack growth. *Engineering Fracture Mechanics* **26**.6 (1987), pp. 841–850.

[22] G. A. Maugin. Material forces: concepts and applications. *Applied Mechanics Reviews* **48**.5 (1995), pp. 213–245.

[23] M. E. Gurtin and P. Podio-Guidugli. Configurational forces and a constitutive theory for crack propagation that allows for kinking and curving. *Journal of the Mechanics and Physics of Solids* **46**.8 (1998), pp. 1343–1378.

[24] J. Brouzoulis and M. Ekh. Crack propagation in rails under rolling contact fatigue loading conditions based on material forces. *International Journal of Fatigue* **45** (2012), pp. 98–105.

[25] D. Rozumek and E. Macha. A survey of failure criteria and parameters in mixed-mode fatigue crack growth. *Materials Science* **45**.2 (2009), pp. 190–210.

[26] C. Li. Vector CTD criterion applied to mixed mode fatigue crack growth. *Fatigue & Fracture of Engineering Materials & Structures* **12**.1 (1989), pp. 59–65.

[27] P. E. Bold, M. W. Brown, and R. J. Allen. A review of fatigue crack growth in steels under mixed mode I and II loading. *Fatigue & Fracture of Engineering Materials & Structures* **15**.10 (1992), pp. 965–977.

[28] P. Zerres and M. Vormwald. Review of fatigue crack growth under non-proportional mixed-mode loading. *International Journal of Fatigue* **58** (2014), pp. 75–83.

[29] D. Floros, A. Ekberg, and F. Larsson. Evaluation of mixed-mode crack growth direction criteria under rolling contact conditions. *Wear* **448-449** (2020), p. 203184.

[30] E. Lansler and E. Kabo. Subsurface crack face displacements in railway wheels. *Wear* **258**.7-8 (2005), pp. 1038–1047.

[31] K. L. Johnson. *Contact mechanics*. Cambridge University Press, 1985.

[32] J. Nielsen and A. Igeland. Vertical dynamic interaction between train and track influence of wheel and track imperfections. *Journal of Sound and Vibration* **187**.5 (1995), pp. 825–839.

[33] S. Timoshenko and J. N. Goodier. *Theory of elasticity*. McGraw-Hill, 1951.

[34] *ABAQUS/Standard user's manual, version 2020*. Dassault Systèmes Simulia Corp., 2020.

[35] *MATLAB 9.7.0.1190202 (R2019b)*. The MathWorks Inc., 2019.